On the modeling of brick-mortar interface

Fazia Fouchal, Frédéric Lebon, Amna Rekik, Isabelle Titeux

Chapter

ON THE MODELING OF BRICK-MORTAR INTERFACE

Fazia Fouchal
GEMH,
Limoges University, IUT Egletons, France.
Frédéric Lebon
LMA, CNRS UPR7051,
Aix-Marseille University, France.
Amna Rekik
PRISME,
Polytech Orléans, France.
Isabelle Titeux
GRESPI, LGC EA4694
Reims University, France.

1. Introduction

Traditionally, for thousand of years, masonry techniques were commonly used for the building of homes, monuments, walls, and retaining walls. Masonry is one of the oldest construction materials. Since masonry is a composite structure, however, failure of these structures will depend on the properties of the materials (mortar, bricks, etc.), as well as on the characteristics of the bonding between the various components. Two main methods of modeling masonry structures have been developed in the literature. The first method involves macroscopic models and homogenization techniques: the wall is assumed to be a single structural element characterized by a non-linear response when it is exposed to external forces. The second method has been developed for predicting the evolution of cracks and damage at the interface brick-mortar or brick-brick. This chapter deals with two families for the modeling of brick-mortar interface. The first part of this chapter deals with the experimental characterization of the materials (bricks and mortar) and the brick-mortar interface. Hereafter, we describe experimental studies on the shear behavior of masonry on the local scale, in the case of two different assemblies composed of two and three full/hollow bricks, with or without confinement. Two other structures are presented: a small wall made by seven bricks

and the classical problem of a small wall under diagonal compression. The second part of this chapter deals with a phenomenological model of interface. The mechanical modeling approach (and in particular the RCCM [10] adhesive model adopted) is first presented. The model is based on the concept of adhesion variable due to Frémond [12]. A variation equation of this variable is introduced and the coefficients are identified experimentally. The numerical procedure used is then described. Lastly, some numerical examples are given and compared with the experimental data. The third part presents a multi-scale model of interface. The method is based on homogenization theories and asymptotic analysis. In the present work, we assume the existence of a third material: the brick-mortar interface, which is considered as a mixture of brick and mortar with a crack density. To obtain the effective properties of the damaged intermediate material, three aim steps are performed. First, we calculate the exact effective properties of the crack-free material using homogenization techniques for laminate composites, and thus define a first homogeneous equivalent medium. In the second step, we assign a crack density to the material. To model the macroscopic behavior of the cracked material, we use the Kachanov model [18] and then define a new homogeneous equivalent medium. Finally, in order to be sandwiched between the brick and mortar, this material is given a small thickness, and its mechanical behavior is derived using asymptotic techniques to shift from the micro to the macro level. A variation law of the crack length is introduced. The numerical procedure used is then described. Lastly, some numerical examples are given and compared with the experimental data.

2. Experimental Study of The Masonry

2.1. Introduction

The first part of this paper is dedicated to the experimental study of the mechanical behavior of the masonry. The experimental studies were performed on the materials and masonry specimens (single, couplet, triplet, wall) composed of full and hollow bricks in order to identify the mechanical behavior of the bricks, mortar and bricks /mortar joint, in particular under shear tests with and without confinement pressure.

2.2. Characterization of Materials

2.2.1. Mortar

The mortar used in this study is a ready-to-use mortar from "Weber and Boutrin" based on sand and cement (ciment is Portland type 52.5). The maximum size of the sand grains is $5\ mm$. The mortar characteristics are given in Table 1.

The standard tests following the EN 196-1 norm [5] were performed to determine the traction and compression strength [1].

The results concerning the flexion and compression limits are summarized in Table 2. The flexion strength is around $4,26MPa$ and the compression strength is around $23MPa$ [1]. The elastic modulus given in [3] is equal to ($4000MPa$).

Table 1. **Characteristics of the mortar**

Granulometry	$0 - 5\ mm$
Dosing of bond / m^3 dry sand	$350\ kg$
Water for mixing	12.5% • $5\ L/$ sack of $40\ kg$ or: • $3\ L/$ sack of $25\ kg$
Density after 28 days	2.25
Contraction after 28 days	0.65

Table 2. **Mechanical characteristics of the mortar**

Nb.	Flexural test		Compression test			
	Traction loading (kN)	Flexion strength (MPa)	Compression loading (kN)		Compression strength (MPa)	
			1^{st} half prism	2^{nd} half prism	1^{st} half prism	2^{nd} half prism
1	1.95	4.56	39.5	36.9	24.7	23.1
2	1.87	4.39	39.2	34.4	24.5	21.5
3	1.69	3.95	33.6	30.7	21.0	19.1
4	1.91	4.47	37.7	44.7	23.5	27.9
5	1.65	3.86	37.3	35.8	23.3	22.4
6	1.85	4.33	31.8	39.5	19.8	24.7
Mean value	1.82	4.26	36.5	37.0	22.8	23.1

2.2.2. Bricks

Full and hollow cooked earth bricks were used for the mechanical tests. The dimensions of each brick are $210\ mm$ (length), $100\ mm$ (width), $50\ mm$ (height). Hollow Bricks are composed with ten holes ($25 \times 25\ mm^2$ in size) arranged in two rows. A compressive standard tests using NF EN 772-1 norm [6] were carried out on a series of three units full/hollow bricks in order to identify the compressive strength, elastic modulus and Poisson coefficient of the masonry units. Bricks are equipped with strain gauges glued in transverse and longitudinal directions (unidirectional compression test) and an extensometric sensor. Compressive load was applied on the upper face of the brick up to failure in two steps: the load was gradually increased as shown in Table 3; half-way to maximum pressure within $1\ min$. The elastic modulus is determined from the strain-stress curve at $30\ \%$ of the ultimate load.

Table 3. **Loading rate**

Expected Strength (N/mm^2)	Loading rate $(N/mm^2)/s$
< 10	0.05
from 11 to 20	0.15
from 21 to 40	0.3
from 41 to 80	0.6
> 80	1.0

Three tests are carried out on each kind of brick [1]. The curve giving the longitudinal deformation with respect to the normal stress and transversal deformation with respect to the normal stress are shown in Figures 1 and 2.

The quantitative data obtained on these mechanical parameters are summarized in Tables 4 and 5.

The experimental results obtained were similar to the mean value recorded by two gauges. The dispersion of the results was very small.

Table 4. Mechanical properties for full bricks

Nb	compression strength (MPa)	Elastic Modulus (MPa)	Poisson Coefficient
1	11.7	9 439	0.13
2	10.2	10 447	0.14
3	13.3	8 429	0.13
Mean value	11.7	9 438	0.13

Table 5. Mechanical properties for hollow bricks

Nb	Compression strength (MPa)	Elastic modulus (MPa)	Poisson coefficient
1	4.4	5 934	0.14
2	4.4	6 737	0.14
3	4.6	5 505	0.12
Mean value	4.46	6 059	0.13

2.3. Mechanical Behavior of Small Masonry Structures Under Shear Loading Without Confinement

2.3.1. Experimental Procedure

In order to determine the influence of the unit volume, two kinds of prism have been tested. The first kind is composed of two bricks, the second one is composed of three bricks (Figure 3). For each kind of unit volume, full or hollow bricks have been used. Mortar joint thickness used for the samples is equal to $10\ mm$. The aim of this experimental study is to determine the shear behavior and the rupture modes at the interface brick/mortar.

Prisms were prepared following the standard NF EN 1052-3 norm [7].

The samples were subjected to a monotonously increasing load until damage occurred [2].

Relative displacement between the loading brick and the unloading brick is measured by extensometric LVDT captors. Test machine and captors are connected with a PC in order to record data during the test notably the longitudinal strain and the applied load data.

Curves giving the shear stress with respect to the relative displacement were plotted that will determine the shear behavior law. The results are presented and commented in the following paragraphs.

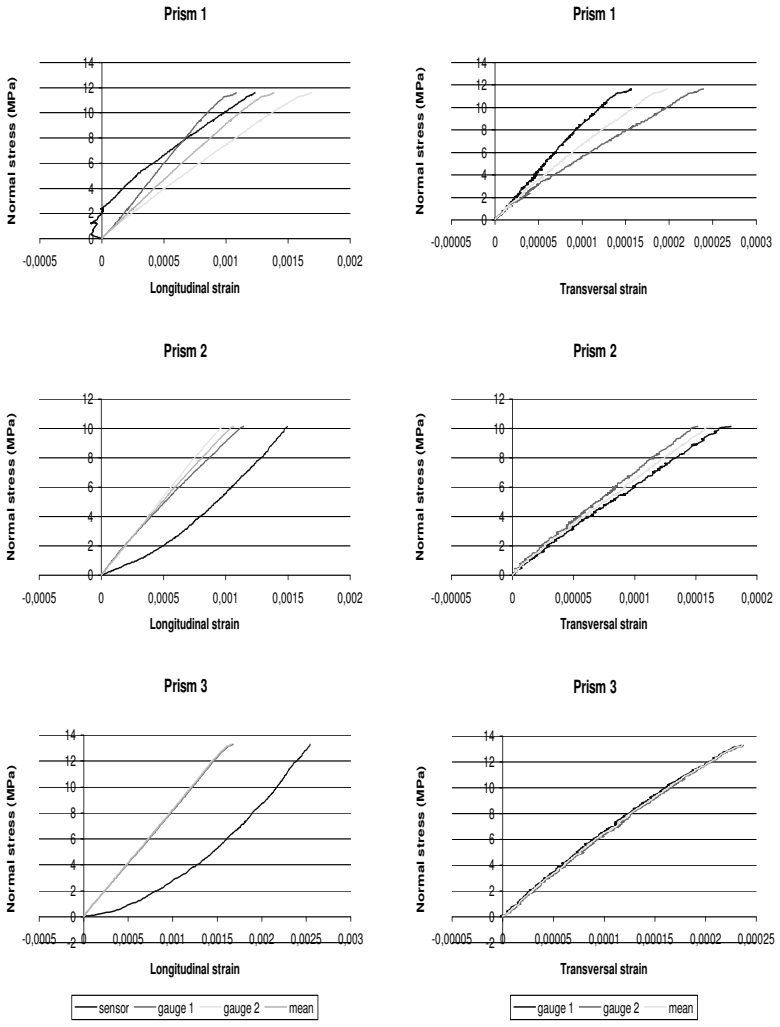

Figure 1. Compression test on full bricks: Elastic modulus and Poisson's coefficient

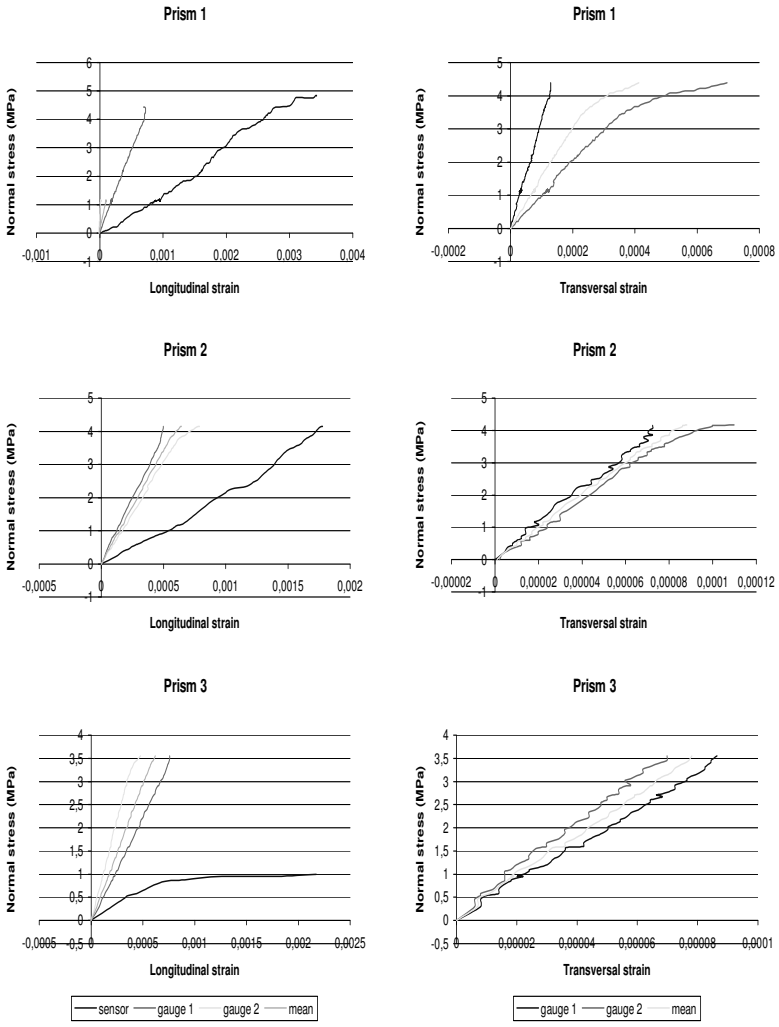

Figure 2. Compression test on hollow bricks: Elastic modulus and Poisson's coefficient

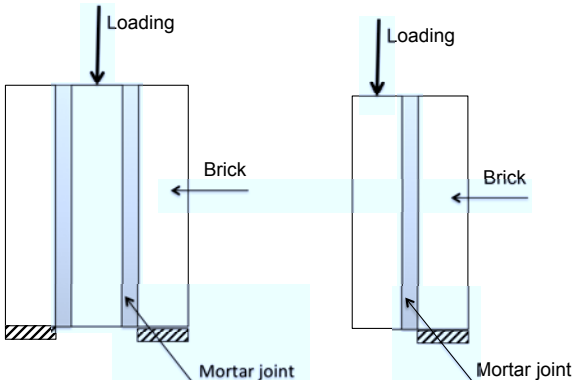

Figure 3. Shear test: (a) Three bricks unit (b)Two bricks unit

2.3.2. Full Bricks

Figure 4 represents the recorded displacements with respect to the shear load $\tau = \frac{F}{A}$ where F is the imposed load on the upper face of the prism and A is the shear surface ($A = hight \times length = 210 \times 100\, mm^2$).

Figure 5 shows the different failure modes obtained under shear test for the full brick prisms.

2.3.3. Hollow Bricks

Figure 6 represents the recorded displacements with respect to the shear load $\tau = \frac{F}{A}$ where F is the imposed load on the upper face of the prism and A is the shear surface ($A = hight \times length = 210 \times 100\, mm^2$).

Figure 7 shows the different failure modes obtained under shear test for the Hollow brick prisms.

2.3.4. Discussions

The experimental studies of different masonry samples presented have shown a nonlinear behavior on the local scale. We have observed a rigid elastic behavior to the rupture. The behavior of the specimen in full bricks is fragile in contrast to the response of the specimen in hollow bricks which is characterized by a softening behavior followed by the sliding movement between the adjacent bricks. The obtained results on hollow bricks samples have shown a wide dispersion. This is due essentially to the nonuniform distribution of the mortars spikes and local defects of the components of bricks masonry. We have noted that the couplet and the triplet samples made by a hollow bricks possess the same behavior. Consequently, the choices of basic cell have no influence on local scale. The rupture modes analysis confirms heterogeneity of masonry structures. This study allows us to identify phenomena that govern the rupture of the masonry at a local scale and to characterize the

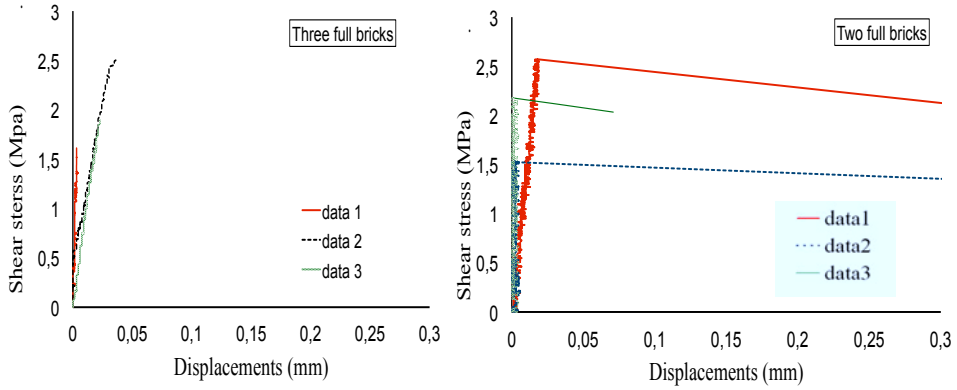

Figure 4. Shear test for full brick prisms

Figure 5. Failure modes - full brick prisms

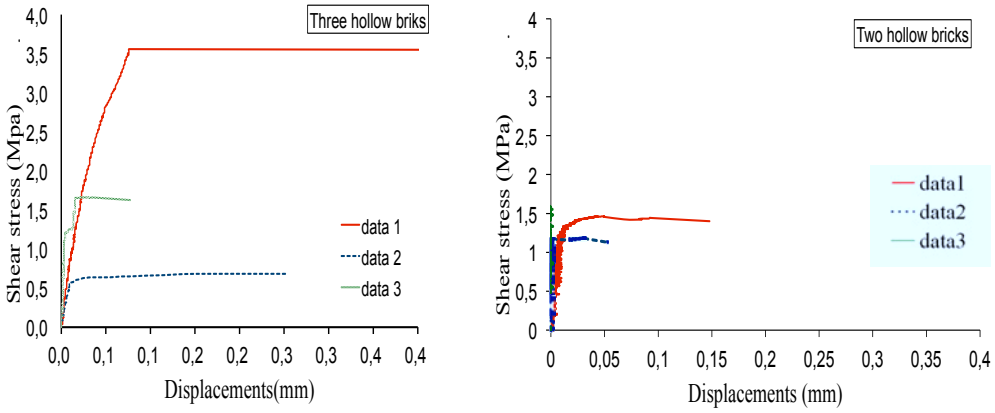

Figure 6. Shear test for Hollow brick prisms

Figure 7. Failure modes - Hollow brick prisms

mechanical properties and the behavior law to take into account in finite elements computations [1] presented in the next section of this chapter.

2.4. Mechanical Behavior of Small Masonry Structures Under Shear Loading With Confinement

Small masonry structures subjected to both shear load and lateral confinement were study in [4]. In this section, we will focus on mechanical tests data obtained in [3, 4]. For this case, the dimensions of hollow ceramic bricks used are $(210 \times 100 \times 50mm^3)$, composed of ten holes. The holes sizes are $25 \times 25\ mm^2$ arranged in two rows. Mean value of compression strength and elastic modulus obtained by the standard compressive test on ten hollow bricks are $13,7MPa$ and $5820MPa$, respectively. Mortar used in this study is a ready-to-use mortar from "Lafarge-LANKO151" based on sand and cement (ciment is Portland type 52.5). The maximum size of the sand grains is $5\ mm$. The mortar characteristics are given in Table 1. Figure 8 presents the samples that were used for the mechanical tests performed according to RILEM recommendations [8]. Eighteen prisms were tested under loads confinement with various values between $0MPa$ and $1.6MPa$. The mechanical behavior of prisms showed in Figure 9 is characterized by a very rigid behavior for elastic domain, with little displacement (order of microns). The softening behavior is observed after the maximum stress followed by sliding movement between adjacent bricks. The confinement stress led to softening behavior in the masonry, when the confinement stress $\sigma = 0MPa$ the failure appears immediately. Identical tests give the same curves but with dispersion on the value of shear stress limit. This difference can be explained by the presence of spikes in the brick holes. Figure 10 show than spicks in the holes prevents brutal failure of a shearing prism and conditioned the shear stress limit. Analysis of the interface brick-mortar damage can identify two phenomena which are responsible for the prisms failure.

- spicks shearing
- rupture of the inner walls of the brick

The stress confinement σ has no significant influence on the evolution of limit shear stresses. The experimental data of these tests identifies three main values: $1.63MPa$, $1.85MPa$ and $2.2MPa$, respectively, as the lower, middle, and maximal value.

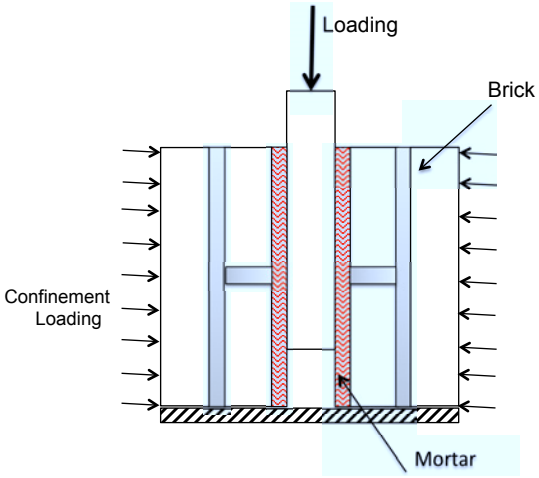

Figure 8. Experimental shear test: Hollow bricks [3]

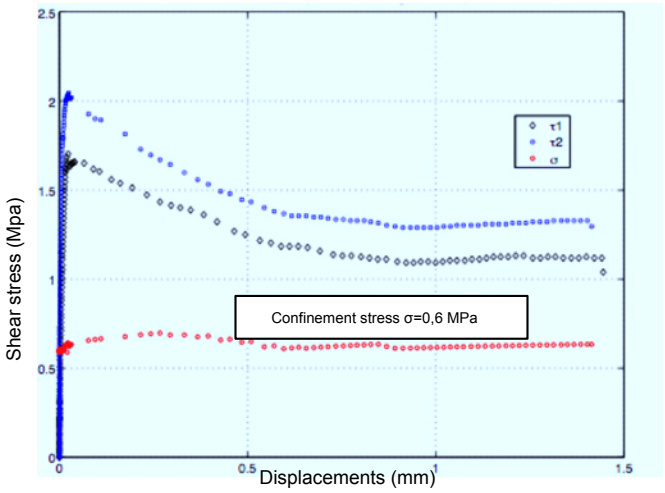

Figure 9. Measured Shear-displacement diagram for test $\sigma = 0,6MPa$ confinement stress

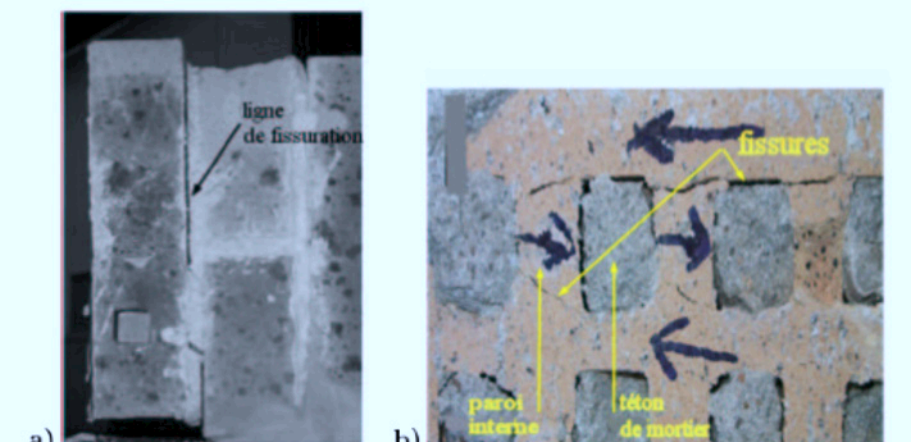

Figure 10. Failure modes - Hollow brick prisms

2.5. Mechanical Behavior of Small Wall in Diagonal Compression

Now we present the mechanical results of the compression diagonal test obtained on the small wall masonry performed by Gabor [3]. This test can produce a stress and strain state where shear and compression are predominant. It is also possible to reproduce the failure by traction diagonal. Such loads are similar to loading developed in masonry construction subjected to earthquake. Figure 11 shows the experimental device used for this study. Test is monotonous with controlled loading. Wall dimensions are $870 \times 840 \times 100mm^3$; it is made with the same materials presented in prevoius paragraphs as recommended by RILEM [9]. Walls were tested after 28 days after manufacture. Mortar joint thickness is $10mm$. Three walls were created in this work.

To obtain a good load level during a test and produce a global stress - strains state on masonry in the aim to produce a failure on the wall diagonal corners have been set by a metal shoe filled with concrete. Two different values for metal shoe length were considered in mechanical test. The first is equal to $L/10$ the second one is equal to $L/6$. The first wall was tested with the first value in the second and third walls were tested with the second value.

State strain was measured by the compression (resp. tense) diagonal shortening (resp. elongation). Extensometric LVDT captors were fixed on the twice diagonal directions in order to measure the displacement between two points in the same diagonal.

Curves load-strain Figures 12 obtained experimentally can evaluate global response of masonry wall.

In the first test with $L/10$, a failure was produced by the sliding and crushing of the joints in support zone. The maximum load is equal to $160kN$ and failure is located on the three rows. In this case, the embedding conditions of corners wall " metal shoe length " cannot distribute the load in wall satisfactorily.

Figure 11. Experimental device for compression diagonal test

Cracks did not appear in the central zone of wall after test. Evolution load with respect to the strains Figure 12 identifies a elastic linear behavior of wall except zone support.

In order to avoid these failure modes, the boundary conditions were changed to a new length support equal to $L/10$ was considered for next tests. In this case, failure was observed on central zone wall following the diagonals. Cracks were crossing both bricks and mortar joint, see Figure (13).

Elastic linear behavior was observed in analysis of the curves r_1 and r_2 (Figure 12). The first wall is characterized by an elastic post level which appears at 90% of the limit load that predicts a degradation of mechanical properties. Maximal load for the first wall is equal to $215,3kN$ and $251,8kN$, for the second. Strains and loading measured are summarized in Table 6.

Table 6. Compression diagonal test data $L/6$

Wall and diagonal		Load (kN)		Strains (mm/mm)	
Test	Diagonal	Elastic	Maximal	Elastic	Maximal
r1	Compressive	188,3	215,3	415	520
	tense			98	190
r2	Compressive	251,8	215,8	670	700
	tense			170	220

Results shows a gap of 17% between maximal load obtained on the last two walls tested. This difference can be explained by the internal structure wall. The strength is governed essentially by the brick-mortar interfaces. That is confirmed by the experimental study presented in the first section of this work.

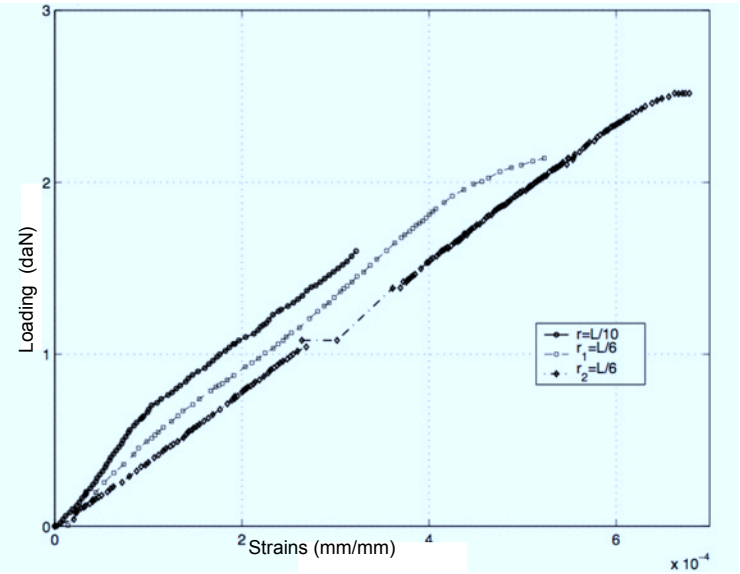

Figure 12. Compression diagonal test - Strain of compressive diagonal

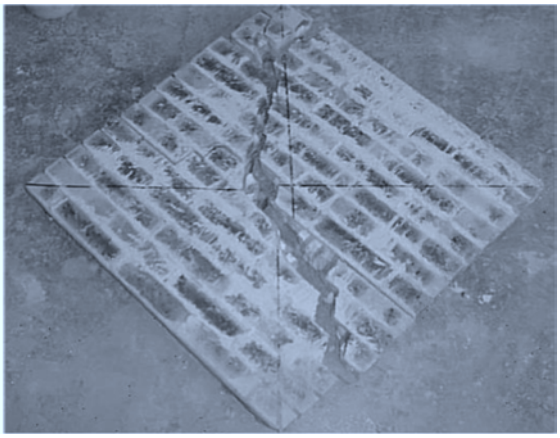

Figure 13. Cracking and failure of the wall

3. Phenomenological Model of Interface

3.1. Introduction

In this section, we are interested in the mechanical behavior of the interfaces for masonry modeling structures when using the materials and interfaces characteristics that were determined experimentally in the previous section [2, 1]. First, RCCM model [10, 11] that is based on the adhesion intensity is presented. Second, this model was adopted to describe the interfaces between mortar and full or hollow bricks in particular; in this case, triplet assemblies subjected to shear loading. The mechanical behavior predicted by this model is compared with the previously obtained in the experimental data.

3.2. Presentation of RCCM Model

RCCM adhesion model was adopted to model the mortar/brick interfaces [10, 11]. This model combines the unilateral contact conditions (non-penetration between the mortar and the brick) with friction and adhesion between two deformable solids. The local constitutive equations required for this model are deduced from thermodynamic considerations and based on a material surface hypothesis for the contact zone. The basic idea underlying this model is to introduce a new state variable describing the contact state. This adhesion intensity variable, denoted β, was initially introduced by [12]. This variable gives the relative proportion of the active links between two bodies in contact. This variable is chosen as:

- $\beta = 1,$ total adhesion
- $0 < \beta < 1,$ partial adhesion
- $\beta = 0,$ no adhesion

We are working in the framework of the contact between two deformable solids. The contact could be defined by a punctual correspondence between two surfaces in contact Γ_c^1 and Γ_c^2 of the domains Ω^1 and Ω^2 of R^d $(d = 2, 3)$, respectively. At initial time $t = t_0$, we assume that $\Gamma_c = \Gamma_c^1 = \Gamma_c^2$. The relative displacement between two points located on the two surfaces in contact is denoted by $[u]$ with $[u] = u^1 - u^2$. Let R be the density of the contact forces. We take n^1 and n^2 to denote the external unit normal vectors to the boundaries of the two domains. The decomposition into normal and tangential parts is written:

$$[u] = [u_N]n^1 + [u_T] \quad with \quad [u_N] = [u].n^1 \tag{1}$$

$$R = R_N n^1 + R_T \quad with \quad R_N = R.n^1 \tag{2}$$

The state variables for the thermodynamical description of this model are:

- Strain tensor $e = (e_{ij})$
- Displacement jump $[u]$

- Intensity of adhesion β

b is taken to denote the adhesion viscosity coefficient, w to denote the Dupré energy, μ to denote the friction coefficient and C_N (resp. C_T) to denote the initial normal (resp. tangential) stiffness of the interface. In what follows, $\dot{f}$ denotes the rate of the function f. The constitutive equations of the interface are given by the following equations, as based on state laws and complementarity laws:

Unilateral Contact With Adhesion

$$R_N - C_N[u_N]\beta^2 \geq 0; \quad [u_N] \geq 0; \quad (R_N - C_N[u_N]\beta^2)[u_N] = 0 \tag{3}$$

Friction With Adhesion

$$\begin{array}{rcll} ||R_T - C_T[u_T]\beta^2|| & \leq & \mu|R_N - C_N[u_N]\beta^2| & \\ ||R_T - C_T[u_T]\beta^2|| & < & \mu|R_N - C_N[u_N]\beta^2| & \Rightarrow \quad [\dot{u_T}] = 0 \\ ||R_T - C_T[u_T]\beta^2|| & = & \mu|R_N - C_N[u_N]\beta^2| & \Rightarrow \quad \exists\lambda \geq 0, \\ & & & [\dot{u_T}] = \lambda(R_T - C_T[u_T]\beta^2) \end{array} \tag{4}$$

Evolution of The Intensity of Adhesion

$$\begin{array}{rcll} b\dot{\beta} & = & -(w - (C_N[u_T]^2 + C_T|[u_T]|^2)\beta)^- & if \quad \beta \in [0,1[\\ b\dot{\beta} & \geq & -(w - (C_N[u_T]^2 + C_T|[u_T]|^2)\beta)^- & if \quad \beta = 1 \end{array} \tag{5}$$

Note that if there is no adhesion ($\beta = 0$), this model involves the classical Signorini-Coulomb problem.

A graphic interpretation of the tangential part of this RCCM model given in figure 14 shows the changes with time in the tangential forces depending on the tangential displacement jump. The changes in β lead to irreversible effects. If β decreases, the adhesive forces will decrease and eventually disappear. In the case of pure traction ($[u_N] > 0$), the adhesion resistance ($R_N = C_N[u_N]\beta^2$) is activated (elasticity without damage). β decreases when the displacement becomes sufficiently large for the elastic energy to become larger than the adhesion limit w.

3.3. Implementation of RCCM Model

The numerical problem was solved using the open computer code LMGC90 (http://www.lmgc.univ-montp2.fr/ dubois/LMGC90/). This code is a numerical platform dedicated to the modeling and simulation of dynamic multibody problems. Problems were approached in the general framework of dynamics. Discretized equations of the problem P are written as:

$$\begin{array}{rcl} M\ddot{q} & = & F(q,\dot{q}) \ + \ P(t) \ + \ r, \\ & + & \text{interface conditions} \\ & + & \text{initial conditions and boundary conditions} \end{array} \tag{6}$$

with q is a parametrization of the system (degrees of freedom), M is the mass matrix, $F(q,\dot{q})+P(t)$ are the internal and external loading vectors, r is the vector of contact forces.

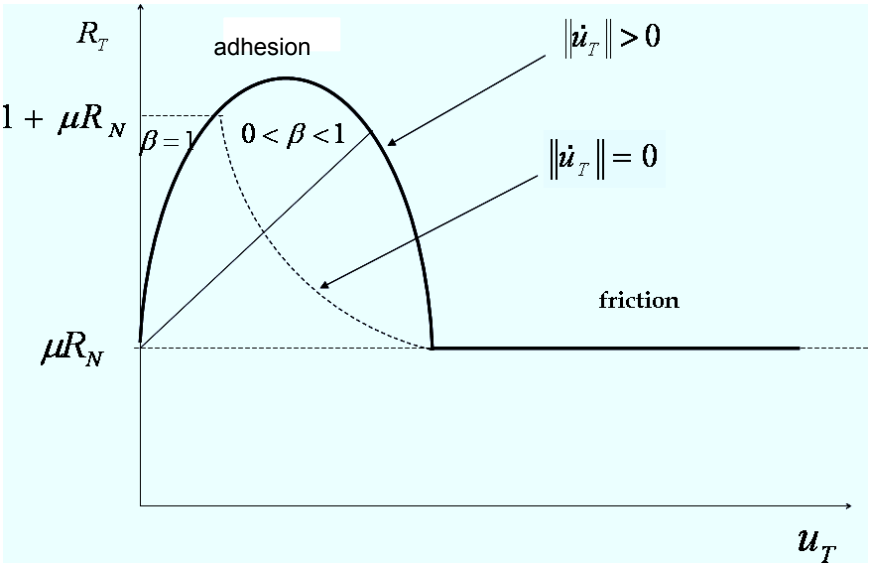

Figure 14. *Normalized tangential forces against normalized tangential jump of displacement*

Problems were usually approached using θ-methods and the Non-Smooth Contact Dynamics (NSCD) method [13, 14, 15]. Due to the contact conditions, a fairly small time-step is chosen and the problem is condensed in the local frame associated with the contact nodes. The local problem is solved using a non-linear Gauss-Seidel method.

The interface is governed by the RCCM law as presented earlier in this chapter. Contact between bodies is defined by contact nodes. Contact nodes are located between two nodes in the mesh of an element in contact at distances of 0.2 and 0.8, respectively, along each segment in contact (figure 15).

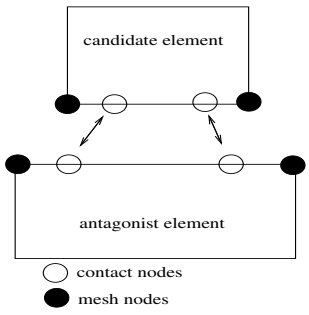

Figure 15. *Position of contact nodes between two bodies*

In this procedure, the bodies (bricks and mortar) are modeled using $Q4$ quadrangular finite elements. The numerical tests are performed with a constant time step equal to $\Delta t =$

$0.5 * 10^{-3}\ s$. The computations require 2000 increments in order to reach values resembling the experimental data, and θ (in the time integration method) is fixed and taken to be equal to 0.55.

3.4. Numerical Results: Mechanical Behavior of Small Masonry Structures Under Shear Loading

In this section, numerical simulations carried out using LMGC90 are presented. In particular, this study deals with various structures (triplets and couplets consisting of full or hollow bricks) previously studied [2, 1] and presented in the first section. It is attempted to model the same conditions as those pertaining in the experimental tests, in terms of the geometries, mechanical characteristics, boundary conditions, and loading conditions. The problems are treated under quasi-static conditions, adopting the plane strain hypothesis. For the sake of simplicity, the parameters used for the computations are: $\mu = 0.2, b \approx 0, w = 0.9\ J/mm^2$. Coefficients C_N and C_T, the normal and tangential stiffness of the interface, will be determined in the following sections. These parameters will be obtained by comparing the experimental and numerical data.

The mechanical characteristics of the materials are as follows Table 7:

Table 7. **Characteristics of Mortar and Bricks**

Materials	Young's modulus MPa	Poisson's ratio
Mortar	4 000	0.3
Full bricks	9 439	0.13
Hollow bricks	6 058	0.13

3.4.1. Full Brick Triplets

In [2], we noted the occurrence of two kinds of fracture processes:

1. The fracture occurs along the interface (tests N1 and N4)
2. The fracture begins along the interface and propagates into the mortar (tests N2 and N3).

Fracture along the interface The experimental data used here was published in [2]. The mesh consists of 130 $Q4$ finite elements. For the sake of symmetry, only the half-structure is considered. The loading on the upper part ranges from 0 to 53 kN. The first step here consists in determining the stiffness values of the interface, C_N and C_T. Various results are presented in figure 16 on pairs of C_N and C_T. The global behavior can be seen to depend strongly on C_N and C_T. The rigidity of the assembly depends mainly on the interface stiffness. Since the problem is highly nonlinear, even small perturbations in the stiffness coefficients can greatly affect the numerical responses.

The results shown in figure 17 were obtained in tests numbers 1 and 4, and are most encouraging, since the general shape of the curves is similar to that of the experimental

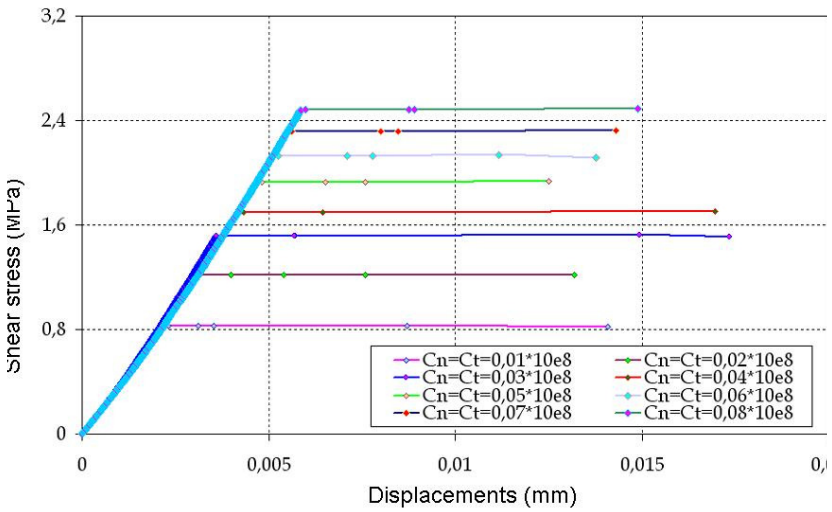

Figure 16. Influence of parameters C_N and C_T on the behavior of full brick triplets

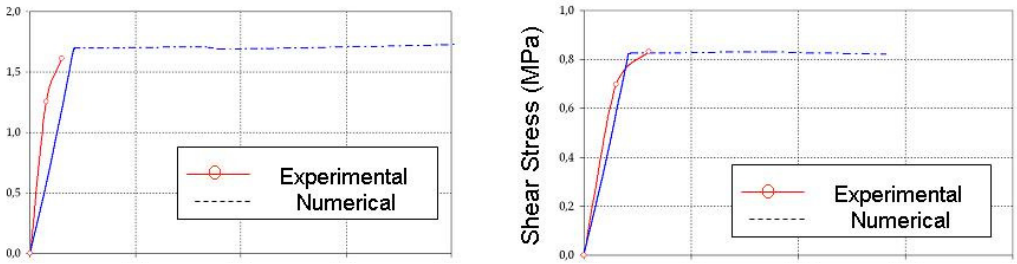

Figure 17. Shear tests: tests N1 ($C_N = C_T = 4\ 10^6 N/mm^3$) and N4 ($C_N = C_T = 10^6 N/mm^3$)

ones. This confirms that the model accounts accurately for the mechanical behavior of the interface. This is also confirmed by the rupture modes obtained numerically (see figure 18). The variations in the shear stresses σ_{xy} show that the stress concentration develops in the regions containing the discontinuities, or more specifically, at the level of the interface.

Cracks developing into the mortar We now take the case where the interface and the mortar are fractured together. The results of the tests performed in this case are not as satisfactory as the previous ones. In this experimental part of this study, we note that the cracks started to develop at the brick-mortar interfaces but continued into the mortar itself

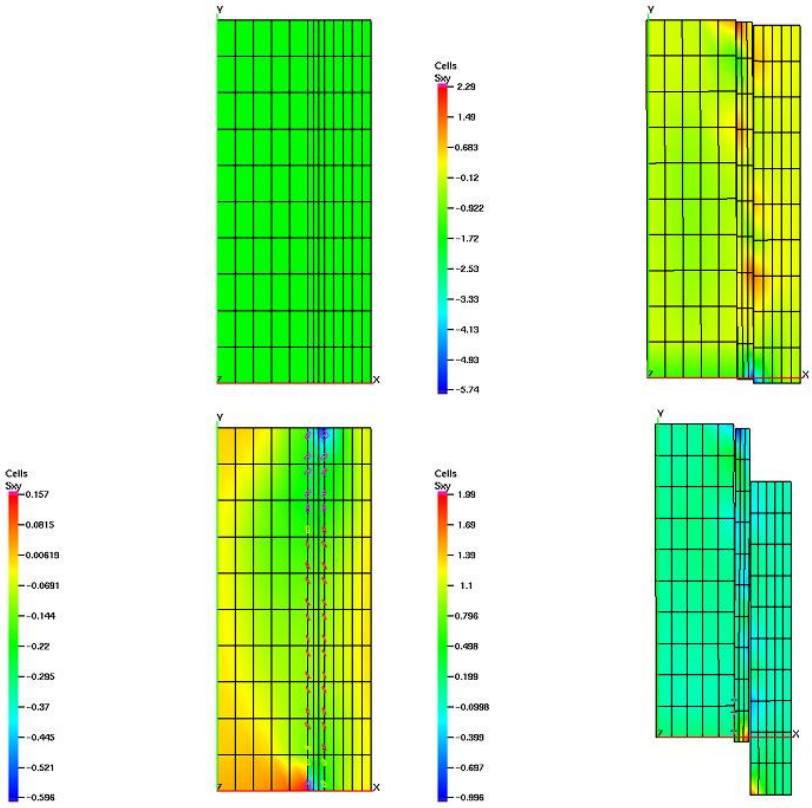

Figure 18. Shear stress in full brick triplets at steps 0, 100, 207 and 208

(tests 2 and 3).

It is therefore proposed to introduce the damage to the mortar, using a cohesive zone model. The mortar is split into sub-bodies. Each sub-body is meshed using a quadrangular mesh with $Q4$ finite elements (figure 19). The contact between sub-bodies is governed by the RCCM model. We take $adh1$ and $adh2$ to denote the law of adherence at the mortar/mortar and the brick/mortar interface, respectively (figure 19).

It can be seen from figure 20 that the behavior of the structure is sensitive to changes in the stiffness coefficients.

The numerical results are in good agreement with the experimental data from the qualitative point of view. They show the degradation of the rigidity induced by the propagation of the crack into the mortar in the two experimental tests 2 and 3 (figure 21). The model predicted the similar occurrence of cracks in the mortar joint to those observed in practice (figure 22).

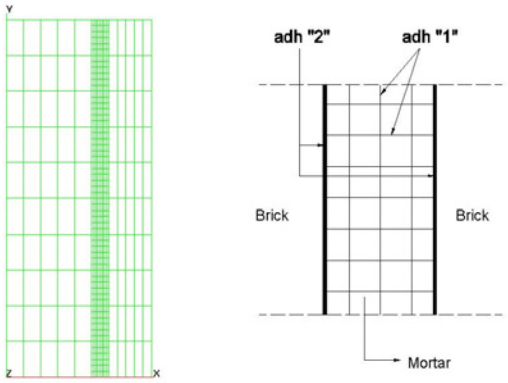

Figure 19. Full brick triplets: a) Mesh with cohesive mortar b) Mortar/mortar and mortar/brick adhesion

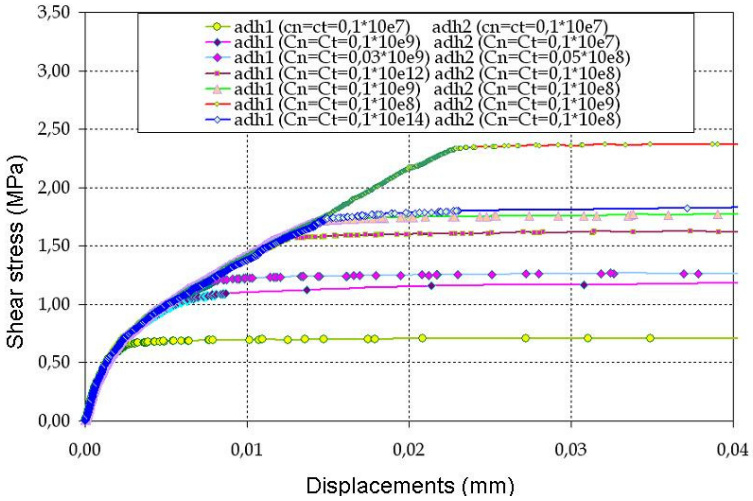

Figure 20. Influence of the stiffness parameters on the behavior of the structure (triplets with a cohesive zone)

3.4.2. Hollow Brick structures

In the case of hollow brick structures, the experimental data show that the behavior of the material at the interface is quite different between the hollow parts of the brick and the full parts. At the level of the hollow parts, spikes of mortar penetrate into the voids of the brick. It is therefore necessary to distinguish between two zones: the zone (adh1) corresponding to the mortar/brick interface as in the case of full brick structures; and the second zone (adh2) corresponding to the spikes. Figure 23 shows these two zones.

By suitably choosing the stiffness coefficients, this strategy makes it possible to ap-

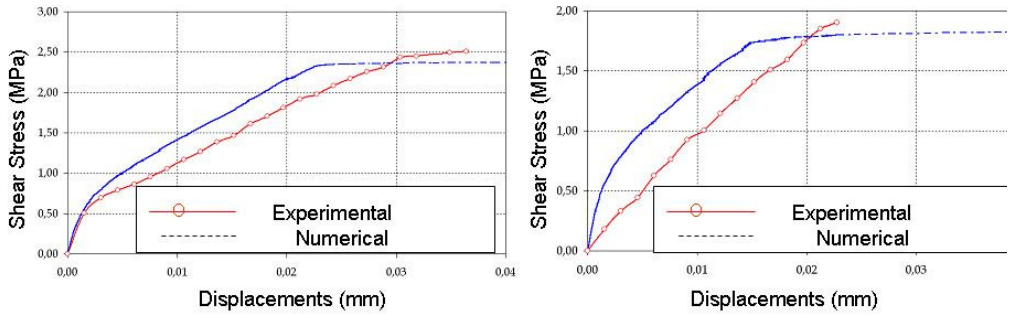

Figure 21. Results of numerical shear tests: tests N2 (adh1: $C_N = C_T = 10^7 N/mm^3$, adh2: $C_N = C_T = 10^8 N/mm^3$) and N3 (adh1: $C_N = C_T = 10^9 N/mm^3$, adh2: $C_N = C_T = 10^8 N/mm^3$)

proach the experimental results, as can be seen from figure 24. However, it is necessary to find several coefficients, which reduces the efficiency of the method. This situation could possibly be improved by averaging the two zones, but this approach has not yet been attempted. The changes with time in the shear stress and in the deformed structure are shown in figure 25.

3.5. Partial Conclusion

The adhesion model presented here was successfully used to simulate the experimental tests described in [1, 2], which provided the coefficients required to model the interface: stiffness parameters, viscosity coefficient, Dupré's energy and friction coefficient. The model is sensitive to these characteristics but the results obtained are in line with the experimental data.

The two kinds of rupture modes observed experimentally were described using two different adhesive characteristics. It was thus possible to model the fracture process that occur along the interface as well as where it involves mortar.

Structures composed of hollow bricks can also be modeled in this way using two adhesive characteristics. In particular, the model was used here to study the fracture process when it occurs along the interface of a small structure that consists of three hollow bricks. Further studies are now required on the fracture processes crossing the mortar in structures of this kind.

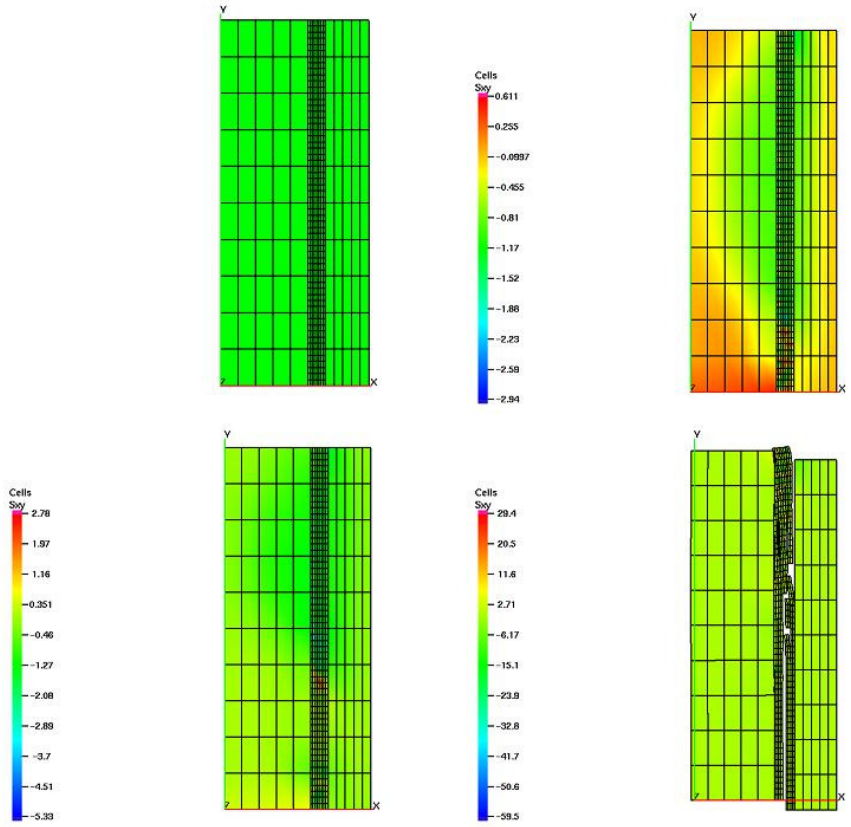

Figure 22. Shear stress in full brick triplets at steps 1, 350, 360 and 371 (cohesive zone)

4. A Multi-Scale Model for Interface Law

4.1. Introduction

In this part of the paper, one presents a multi-scale model of interface [16, 17]. The method is based on homogenization theories and asymptotic analysis. In this context, we assume the existence of a third material: the brick/mortar interface, which is considered as a mixture of brick and mortar with a crack density. To obtain the effective properties of the damaged intermediate material, three steps are performed. First, we calculate the exact effective properties of the crack-free material using homogenization techniques for laminate composites, and thus define a first homogeneous equivalent medium. In the second step, we assign a crack density to the material. To model the macroscopic behavior of the cracked material, we use the Kachanov [18] model and then define a new homogeneous equivalent medium. Finally, in order to be sandwiched between the brick and mortar, this material is given a small thickness, and its mechanical behavior is derived using asymptotic techniques to shift from the micro to the macro level. A variation law of the crack length is introduced. The numerical procedure used is then described. Lastly, some numerical examples are given and compared with the experimental data.

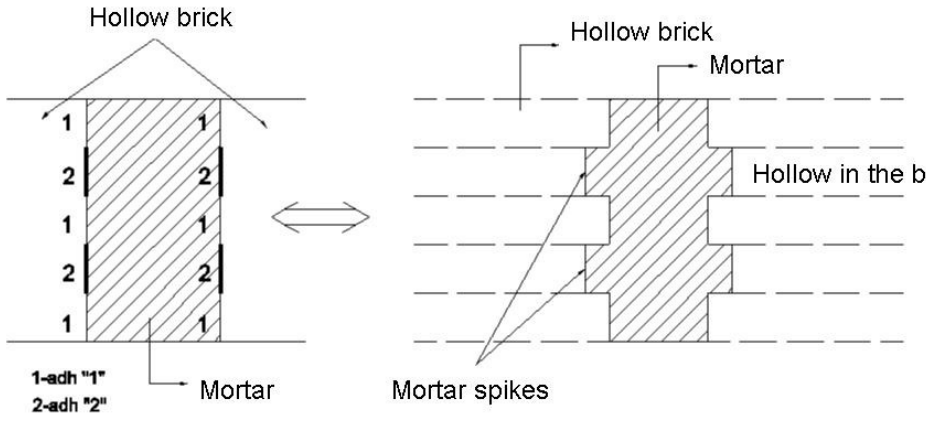

Figure 23. Mortar spike modeling

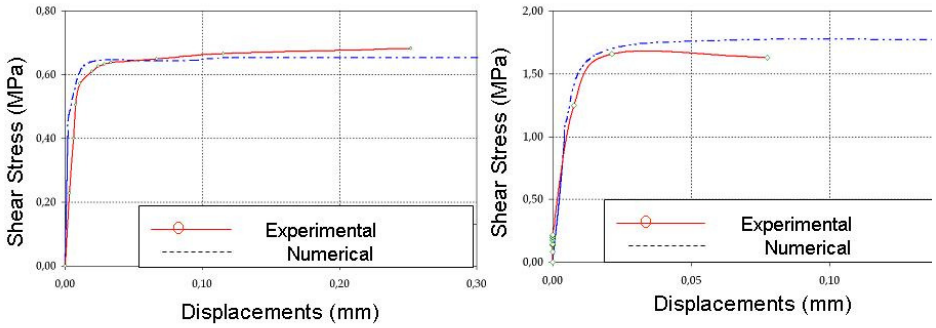

Figure 24. Results of numerical shear tests (hollow bricks): tests N2 (adh1: $C_N = C_T = 2\ 10^6 N/mm^3$, adh2: $C_N = C_T = 4\ 10^7 N/mm^3$) and N3 (adh1: $C_N = C_T = 2.5\ 10^7 N/mm^3$, adh2: $C_N = C_T = 1.5\ 10^8 N/mm^3$)

4.2. Principle of the Model

The procedure used in this paper is summarized in figures 26 and 27.

1. In the first step, we consider the masonry made by bricks and mortar at a local level

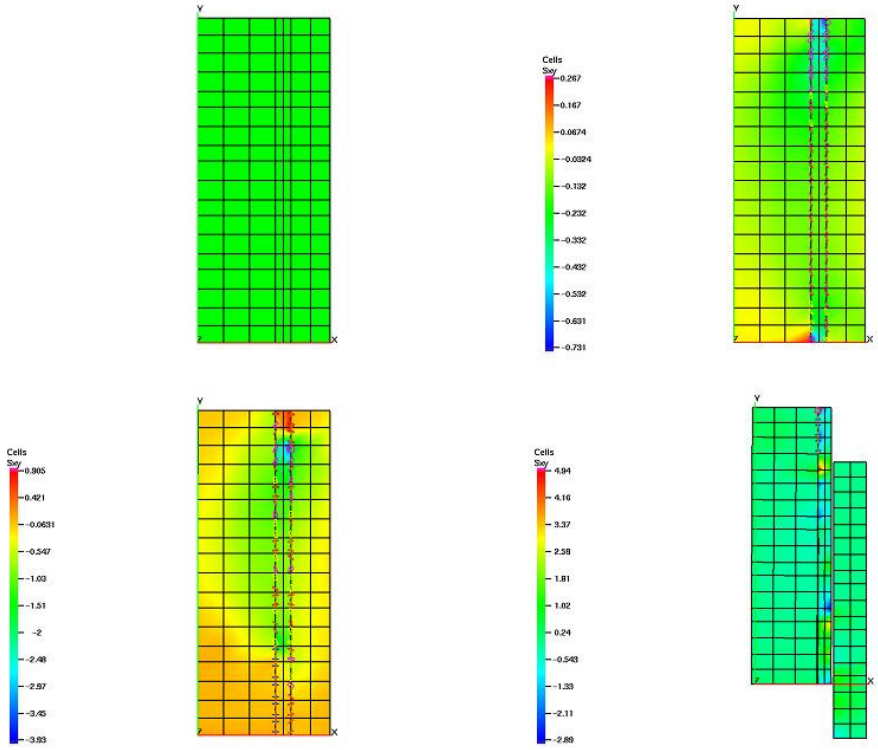

Figure 25. Shear stress in hollow brick triplets atsteps 1, 53, 191, and 196

(Z+1). The brick and mortar are considered as elastic, homogeneous and isotropic materials. The material characteristics are given in former sections.

2. At its local level, an inter-phase is considered a mixture of brick and mortar (Z+2). In order to simplify, we consider the composite inter-phase as stratified.

3. The stratified is homogenized using classical theory of homogenization (H1). A new material is obtained which is transversely isotropic [18]. The new material characteristics are obtained directly from the materials characteristics of brick and mortar.

   The constitutive equation for each material is given by:

$$\varepsilon_{ij}^c = S_{ijkl}^c \sigma_{lk}^c = \frac{1+\nu^c}{E^c}\sigma_{ij}^c - \frac{\nu^c}{E^c}\sigma_{kk}^c \delta_{ij} \tag{7}$$

   where S^c, E^c, and ν^c are respectively the compliance tensor, the Young's modulus and the Poisson ratio of phase c ($c = b$ for the brick, $c = m$ for the mortar). ε^c and σ^c are the strain and the stress tensor, respectively.

   The macroscopic behavior law of the laminate brick/mortar reads:

$$\varepsilon = S^0 : \sigma \tag{8}$$

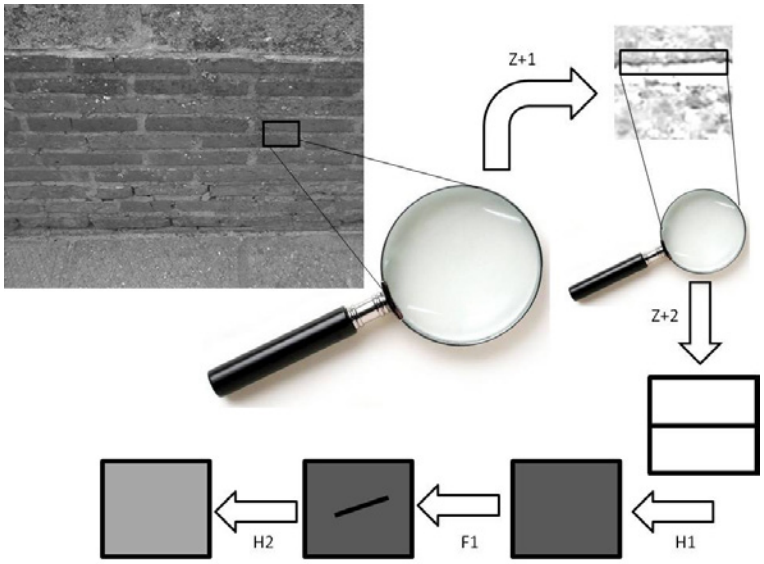

Figure 26. Description of the process 1

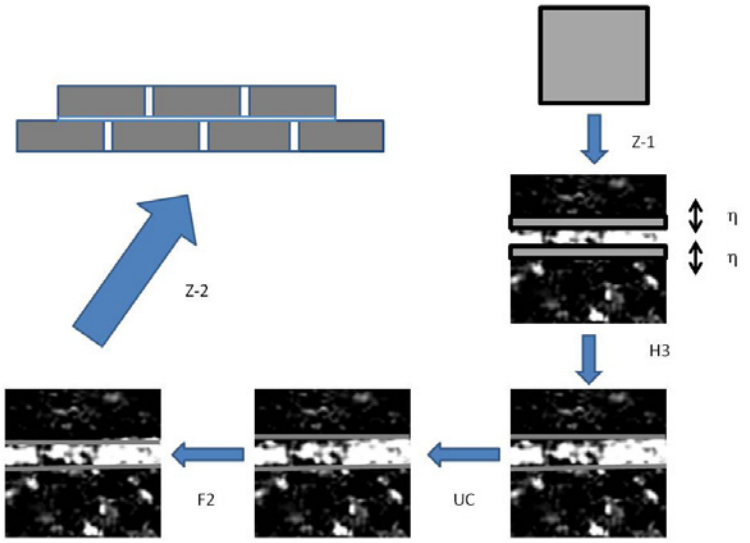

Figure 27. Description of the process 2

where $\varepsilon = \sum_{c=b,\,m} f^c \varepsilon^c = \sum_{c=b,\,m} f^c S^c : \sigma^c$, f^c denotes the volume fractions of phase c, and S^0 is the effective fourth-order compliance tensor of the transversely isotropic stratified. According to the modified Voigt notations, the macroscopic law reads:

$$\begin{pmatrix} \varepsilon_{11} \\ \varepsilon_{22} \\ \varepsilon_{33} \\ \sqrt{2}\varepsilon_{23} \\ \sqrt{2}\varepsilon_{13} \\ \sqrt{2}\varepsilon_{12} \end{pmatrix} = \begin{pmatrix} S^0_{1111} & S^0_{1122} & S^0_{1133} & 0 & 0 & 0 \\ S^0_{1122} & S^0_{1111} & S^0_{1133} & 0 & 0 & 0 \\ S^0_{1133} & S^0_{1133} & S^0_{3333} & 0 & 0 & 0 \\ 0 & 0 & 0 & 2S^0_{1313} & 0 & 0 \\ 0 & 0 & 0 & 0 & 2S^0_{1313} & 0 \\ 0 & 0 & 0 & 0 & 0 & S^0_{1111} - S^0_{1122} \end{pmatrix} \begin{pmatrix} \sigma_{11} \\ \sigma_{22} \\ \sigma_{33} \\ \sqrt{2}\sigma_{23} \\ \sqrt{2}\sigma_{13} \\ \sqrt{2}\sigma_{12} \end{pmatrix} \tag{9}$$

4. We introduce a crack which is representative of the cracks included in the new material (F1). The crack is represented by its average (half-)length l and its average direction ϕ.

5. The cracked material is homogenized using the Kachanov theory [18] (H2). In this theory, the crack is approximated by an elliptic crack. Approximated material characteristics are obtained depending on the length and direction of the crack, and the mechanical characteristics of the brick and mortar. The average strain ε in a solid with one crack can be written in the form:

$$\varepsilon = S : \sigma = S^0 : \sigma + \frac{l}{A}(n \otimes < b > + < b > \otimes n) = (S^0 + \Delta S) : \sigma \tag{10}$$

where S is the effective compliance tensor of the cracked material, $< b >= n.\sigma.B$ is the average displacement discontinuity (COD) vector of the crack, B is the COD tensor of the crack, n is the normal to the crack and A is the area of the representative 2D-domain.

In the plane (e_1, e_3) of the elementary volume, the tensor B is given by:

$$B = (C(1-D)e_1 \otimes e_1 + C(1+D)e_3 \otimes e_3)l \tag{11}$$

where

$$\begin{cases} C = \dfrac{\pi}{4} \dfrac{\sqrt{E^0_1} + \sqrt{E^0_3}}{\sqrt{E^0_1 E^0_3}} \left(\dfrac{1}{G^0_{13}} - 2\dfrac{\nu^0_{13}}{E^0_1} + \dfrac{2}{\sqrt{E^0_1 E^0_3}} \right)^{\frac{1}{2}} \\ D = \dfrac{\sqrt{E^0_1} - \sqrt{E^0_3}}{\sqrt{E^0_1} + \sqrt{E^0_3}} \end{cases} \tag{12}$$

and E_1^0, E_3^0, ν_{13}^0 and G_{13}^0 are given by:

$$\begin{cases} E_1^0 = \dfrac{1}{S_{1111}^0} \\ E_3^0 = \dfrac{1}{S_{3333}^0} \\ \nu_{13}^0 = -\dfrac{S_{1133}^0}{S_{1111}^0} \\ G_{13}^0 = \dfrac{1}{S_{1313}^0} \end{cases} \tag{13}$$

The tensor ΔS is given by:

$$\Delta S = \frac{2l}{A} e_3 \otimes B \otimes e_3 = \frac{2l^2}{A}(e_3 \otimes (C(1-D)e_1 \otimes e_1 + C(1+D)e_3 \otimes e_3) \otimes e_3 \tag{14}$$

The compliance of the cracked material is thus given by:

$$\begin{array}{l} S_{1111} = S_{1111}^0 \\ S_{3333} = S_{3333}^0 + 2\rho C(1+D) \\ S_{1133} = S_{1133}^0 \\ S_{1313} = S_{1313}^0 + 2\rho C(1-D) \end{array} \tag{15}$$

where $\rho = l^2/A$ is the crack density parameter. The elastic constants are given by:

$$\begin{array}{l} E_1 = E_1^0 \\ E_3 = E_3^0/(1 + 2\rho B_{nn} E_3^0) \\ G_{13} = G_{13}^0/(1 + \rho B_{tt} G_{13}^0) \\ \nu_{13} = \nu_{13}^0 \end{array} \tag{16}$$

where

$$\begin{array}{l} B_{tt} = C(1 - Dcos(2\phi))l \\ B_{nn} = C(1 + Dcos(2\phi))l \\ B_{tn} = CDsin(2\phi)l \end{array} \tag{17}$$

6. The cracked material obtained is considered as the inter-phase material (Z-1).

7. The interface law is obtained, considering that the inter-phase is thin (H3). Using asymptotic theory (the thickness of the thin inter-phase η is a small parameter), we obtain an interface law which links the stress vector to the jump of displacement along the interface toward which geometrically inter-phase tends [19]. The stiffness of the interface depends on the material characteristics of the brick and mortar, and on the length and the direction of the crack.

   We take $[u\,]$ to denote the jump along the interface. If the interface is normal to the third direction, we obtain

$$\sigma_{i3} = A_{i3}\,[u_i]$$

The stress vector $\sigma_{.3}$ is linearly linked to the jump of displacement $[u]$. The second order matrix $A_{..}$ is diagonal. The terms C_N and C_T in this matrix, corresponding to the normal and tangential stiffnesses of the interface are given by:

$$\begin{cases} C_N = \bar{C}_{3333}(\eta \to 0) \quad \text{where} \quad \bar{C}_{3333} = \dfrac{C_{3333}}{\eta} \\ C_T = \bar{C}_{1313}(\eta \to 0) \quad \text{where} \quad \bar{C}_{1313} = \dfrac{C_{1313}}{\eta} \end{cases} \tag{18}$$

where the fourth-order stiffness tensor C is the inverse of the compliance tensor S.

In our case $\rho = l^2/\eta\, L_0$, where L_0 denotes the joint length, it can be established that the normal and tangential joint stiffnesses read:

$$\begin{aligned} C_N &= \frac{L_0}{2C(1+D)\, l^3} \\ C_T &= \frac{L_0}{4C(1-D)\, l^3} \end{aligned} \tag{19}$$

We obtain an explicit relation between the stiffness coefficients and the crack length l.

8. Unilateral conditions [20] are introduced (UC). These conditions prevent the penetration between the two adherents (brick and mortar, in our case). In a first approach friction conditions are neglected.

   Let F be the density of the contact forces. We take n^b to denote the external unit normal vector to the boundary of the brick. The displacement and the contact force are decomposed into normal and tangential parts:

   $$[u] = u_N n^b + u_T$$

   with $u_N = [u].n^b$.

   $$F = F_N n^b + F_T$$

   with $F_N = F.n^b$.

   The unilateral contact is given by the following relations

   $$u_N \geq 0,\ F_N - C_N u_N \geq 0,\ u_N(F_N - C_N u_N) = 0. \tag{20}$$

9. An evolution law for the crack length is introduced (F2). In the first step a very simple law is chosen (identified experimentally in practice).

   We take τ to denote the shear stress along the interface.

Table 8. Mechanical properties of the three-fold masonry constituents

Young's moduli (MPa) of full brick	9438
Poisson ratio of full brick	0.13
Young's moduli (MPa) of hollow brick	6059
Poisson ratio of hollow brick	0.13
Young's moduli (MPa) of mortar	4000
Poisson ratio of mortar	0.3

$$\begin{array}{l} \text{if } \tau \leq \tau_c \text{ then } l = l_c \\ \text{if } \tau_c \leq \tau \leq \tau_u \text{ then } l = a\tau + b \end{array} \tag{21}$$

$$\begin{array}{c} a = \dfrac{l_u - l_c}{\tau_u - \tau_c} \\ b = l_u - a\tau_u \end{array} \tag{22}$$

where τ_u, τ_c, l_c and l_u are four given values (In practice, l_c and l_u are identified).

10. The interface law can be used for a structural analysis by finite element (Z-2). In this case, the masonry is made by bricks, mortar, and interface.

4.3. A Numerical Example

We consider two-dimensional masonry structures subjected to shear loading. The obtained numerical results are then compared with experimental data [2]. Two cases are considered: a triplet of full bricks and a triplet of hollow bricks, both subjected to the same nominal loading (with no lateral confinement). Table (8) lists the material properties of the mortar and full bricks used to simulate a triplet of full bricks under the shear loading conditions described (see Fig. 28).

For full bricks, the compliance tensor S^0 therefore reads:

$$10^{-4} \begin{pmatrix} 1.478 & -0.271 & -0.348 & 0 & 0 & 0 \\ -0.271 & 1.478 & -0.348 & 0 & 0 & 0 \\ -0.348 & -0.348 & 1.639 & 0 & 0 & 0 \\ 0 & 0 & 0 & 4.444 & 0 & 0 \\ 0 & 0 & 0 & 0 & 4.444 & 0 \\ 0 & 0 & 0 & 0 & 0 & 3.499 \end{pmatrix} \tag{23}$$

The normal and tangential stiffnesses (N/mm^2) of the interface are given by the following expressions:

$$\begin{array}{rcl} C_N & = & 242365/l^3 \\ C_T & = & 127600/l^3 \end{array} \tag{24}$$

where the direction ϕ is assumed to be equal a zero.

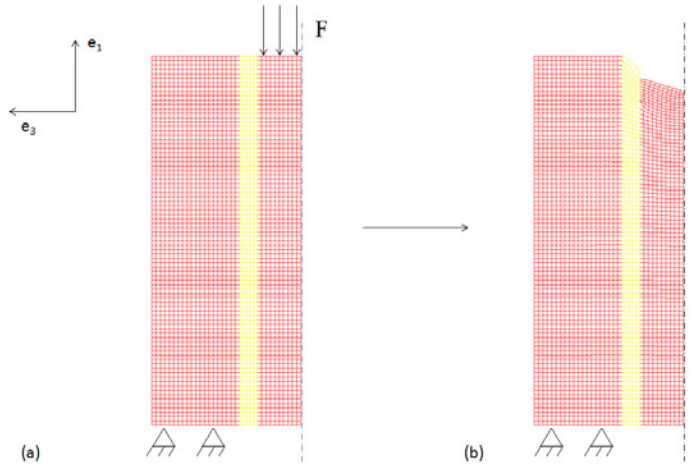

Figure 28. Initial geometrical configuration and loading conditions imposed on the triplet of full bricks (a), deformation of the triplet of full bricks in a shear test (b)

For hollow bricks, the compliance tensor S^0 is written as follows:

$$10^{-4}\begin{pmatrix} 1.973 & -0.396 & -0.456 & 0 & 0 & 0 \\ -0.396 & 1.973 & -0.456 & 0 & 0 & 0 \\ -0.456 & -0.456 & 1.985 & 0 & 0 & 0 \\ 0 & 0 & 0 & 5.115 & 0 & 0 \\ 0 & 0 & 0 & 0 & 5.115 & 0 \\ 0 & 0 & 0 & 0 & 0 & 4.740 \end{pmatrix} \tag{25}$$

The normal and tangential stiffnesses of the interface sandwiched between mortar and hollow brick are given by the following expressions:

$$\begin{aligned} C_N &= 200396/l^3 \\ C_T &= 100490/l^3 \end{aligned} \tag{26}$$

The first step in order to compare experimental data and numerical results is to identify the parameters of the model, in particular the crack length and its evolution [16]. For the fulls bricks, a comparison between experimental data and numerical results is given in figure 29. For the hollow bricks, a comparison is given in figure 30.

4.4. Partial conclusion

The numerical results obtained with the present model match the experimental data and are in good agreement particularly with the test data obtained in previous sections. Thus, the present model, with a simple crack evolution law, seems a good way to provide estimations for the stiffness of masonry interfaces.

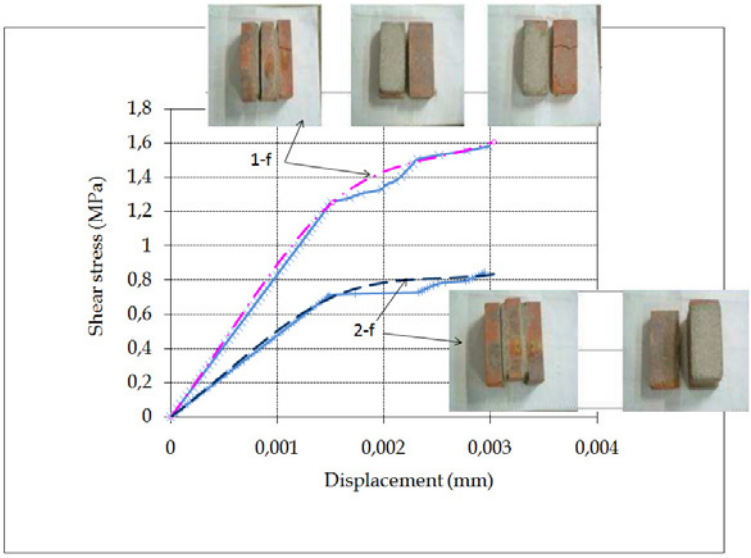

Figure 29. Stress-displacement diagrams of the triplet of full bricks under shear, numerical, and experimental results [16, 17].

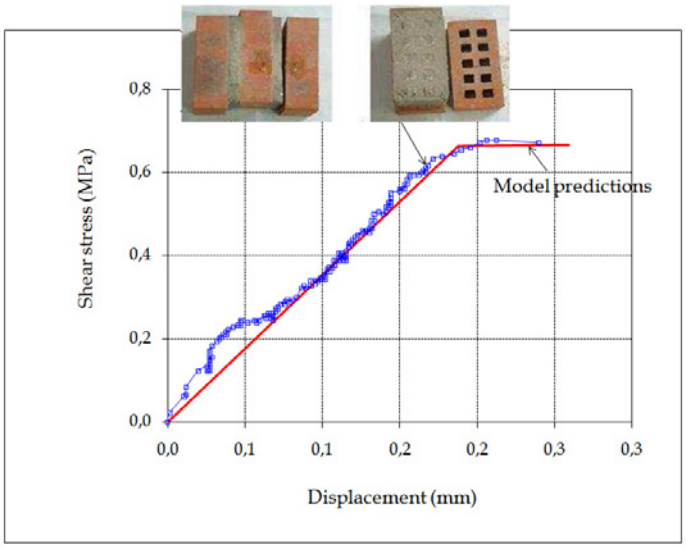

Figure 30. Stress-displacement diagrams of the triplet of full bricks under shear, numerical and experimental results [16, 17].

5. Conclusion

In this chapter, we have presented some experimental data issued from the literature, with a particular focus on small structures and the local behavior of brick-mortar interfaces. We have shown that three aim modes appear in the stress-strain relationship. In the first part, there is a linear (elastic) relationship between the stress and the displacement. After a maximum, in a second step, the stress decreases, due to local damage, to a (quasi) constant value (third part) corresponding to friction.
We have presented two families of models able to predict the behavior of the interface. The first one, phenomenological, is based on the notion of the evolution of the adhesion variable. The second one is based on micromechanics analysis and crack evolution. For these two models, some numerical results are presented and compared with experimental data. The results show the efficiency of these two models.
In the future, various paths are possible. The first one concerns the dynamical aspects that is necessary to take into account, in order to approach earthquakes which generate severe in-plane and out-of-plane forces. It is therefore necessary to generalize our methodology to three-dimensionnal problems. A second possible way concerns the development of efficient numerical schema which is necessary to approach large structures such as monuments. The last line of research could involve the improvement of the models presented in this work to introduce new physical considerations as plasticity, damage evolution, etc.

References

[1] Fouchal, F., Contribution à la modélisation numérique des interfaces dans les structures maçonnées, *PhD Thesis, Reims University*,**(2006)** (in french).

[2] Fouchal, F., Lebon, F., Titeux, I., Contribution to the modeling of interfaces in masonry construction, *Construction and Building Materials*, 23, 2428–2441 **(2009)**.

[3] Gabor, A., Contribution à la caractérisation et à la modélisation des maçonnerie non renforcées et renforcées par matériaux composites, *PhD Thesis, Université Claude Bernard Lyon 1* ,**(2002)**.

[4] Gabor, A., Ferrier, E., Jacquelin, E., Hamelin, P.,, Analysis and modeling of the in-plane shear behavior of hollow brick masonry panels, *Construction and Building Materials* , 20, 308-32, **(2006)**.

[5] NF EN 196-1, Norme Européenne , Norme Française, *Méthodes d'essais des ciments - Partie 1: détermination des résistances mécaniques*, **(2006)**.

[6] NF EN 772-1, Norme Européenne, Norme Française, *Méthodes d'essai des éléments de maçonnerie - Partie 1: détermination de la résistance à la compression*, **(2001)**.

[7] NF EN 1052-3, Norme Européenne, Norme Française, *Méthodes d'essai de la maçonnerie - Partie 3: détermination de la résistance initiale au cisaillement*,**(2003)**.

[8] RILEM (1994b), LUMB5- Short - term shear test for interface between the masonry unit and mortar or moisture - Insulating interlayer. *Technical raport, RILEM*.

[9] RILEM (1994c), LUMB6- Diagonal tensile strength tests of small wall specimens. *Technical raport, RILEM.*

[10] Raous, M., Cangémi, L., Cocou, M., , A consistent model coupling adhesion, friction and unilateral contact, *Computational Methods in Applied Mechanics and Engineering* 177, 383-399 **(1999)**.

[11] Monerie, Y. and Raous, M.,, A model coupling adhesion to friction for the intercation between a crack and a fiber/matrix interface, *Z.A.M.M.* 80, 205-209 (2000).

[12] Frémond, M., Adhérence des solides, *Journal de Mécanique Théorique et Appliquée,* 6, 383-407 **(1987)**.

[13] Moreau, J.J., On unilateral constraints, friction and plasticity. In G. Capriz and G. Stampacchia, eds., in New Variational Techniques in Mathematical Physics, *CIME II ciclo, Edizioni Cremonese*, 175-322, **(1973)**.

[14] Moreau, J.J., Unilateral contact and dry friction in finite freedom dynamics. In J.J. Moreau and P.D. Panagiotopoulos, eds., in Nonsmooth Mechanics and Applications, *CISM Courses and Lectures, vol.302, Springer-Verlag*,**(1988)**, 1-82.

[15] Jean, M., Frictional contact in rigid or deformable bodies: Numerical simulation of geomaterials, *Elsevier Science Publisher, Amsterdam,* **(1995)**, 463-486.

[16] Rekik, A., Lebon, F., Identification of the representative crack length evolution in a multi-level interface model for quasi-brittle masonry, *International Journal of Solids and Structures,* 47, 3011–3021**(2010)**.

[17] Rekik, A., Lebon, F., Homogenization methods for interface modeling in damaged masonry, *Advances in Engineering Software, in press*, **(2011)**.

[18] Kachanov M., Effective elastic properties of cracked solids: Critical review of some basic concepts, *Applied Mechanical Review,* 45, 304–335 ,**(1992)**.

[19] Lebon, F., Rizzoni, R., Asymptotic analysis of a thin interface: The case involving similar rigidity, *International Journal of Engineering Science,* 48, 473–486 **(2010)**.

[20] Lebon, F., Contact problems with friction: Models and simulations, *Simulation Modelling Practice and Theory,* 11, 449–463 **(2003)**.